Master's Thesis

Performance Evaluation of 802.15.4 UWB PHYfor High Speed Data Rate under IEEE Channel Model

Athanasios Vasileiadis

Department of Electrical and Information Technology,
Faculty of Engineering, LTH, Lund University, June 2015.

Performance Evaluation of 802.15.4 UWB PHY for High Speed Data Rate under IEEE Channel Model

Athanasios Vasileiadis

Department of Electrical and Information Technology
Lund University

Advisors: Athanassios Iossifides
Ghassan Dahman

June 29, 2015

Printed in Sweden
E-huset, Lund, 2015

Abstract

In modern day society the increase of data generation and transfer has been an issue that researchers are working on. This generated and shared data might have a different purpose but one thing is certain, the reception. This communication can cover continents, countries, cities or even just a few meters. For the purpose of the later, personal area networks (PAN) have been created with a main focus to lower the energy consumption. The protocol that is created under IEEE is 802.15.4 and it has multiple applications in the context of next generation sensor networks.

This thesis investigates the performance IEEE 802.15.4 UWB PHY for high data rates over IEEE multipath fading channels and introduces receivers aiming to diversity and to mitigate the intersymbol interference (ISI) that might appear. We simulate the protocols highest mandatory data rate over slow, block faded, realistic IEEE channel models such as, residential, office, outdoor and industrial. The simulation includes Reed Solomon (RS) channel coding, optimal successive erasure decoding (SED), and coherent RAKE receivers.

We verify that the selective RAKE (sRAKE) perform better than the non-selective RAKE (n-sRAKE) in all environments and also the increase of fingers is mandatory in order to improve performance. In cases with low number of fingers the ISI mitigation techniques like Maximum-Likehood Sequence Estimator (MLSE) & RAKE combination or Maximum Ration Combining (MRC) ISI cancellation receivers, can provide some gain in large delay spread environments. In cases with high number of fingers the MRC received employs its full diversity since the received power is larger than before. Overall the apply of optimal errors and erasures decoding can further improve the system performance by adding a small gain, lowering existing Bit Error Probability (BEP) even more.

Table of Contents

1 Introduction **1**
- 1.1 Motivation . . . 1
- 1.2 Background . . . 1
- 1.3 Scope of thesis . . . 2
- 1.4 Previous work . . . 2
- 1.5 Methodology . . . 2
- 1.6 Thesis outline . . . 3

2 Description of 802.15.4 UWB PHY **4**
- 2.1 Frame structure and mandatory transmission schemes . . . 4
- 2.2 Information flow . . . 5
- 2.3 Channel coding . . . 6
- 2.4 Modulation and symbol structure . . . 7
- 2.5 Pulse shaping . . . 8

3 Channel Models **10**
- 3.1 IEEE Channel Models . . . 10
- 3.2 Channel statistics . . . 11

4 Receivers **17**
- 4.1 Received signal and reasoning of RAKE implementation . . . 17
- 4.2 MRC RAKE receiver . . . 18
- 4.3 MRC ISI cancellation receiver . . . 19
- 4.4 Maximum Likehood Sequence Estimator (MLSE) & RAKE combination receiver . . . 20

5 Results **23**
- 5.1 Reasoning of sRAKE and NLOS . . . 23
- 5.2 Performance Evaluation under IEEE CM . . . 25

6 Conclusion and future work **30**
- 6.1 Conclusions . . . 30
- 6.2 Future work . . . 31

List of Figures

2.1 Frame structure of 802.15.4 UWB PHY [1]. 4
2.2 Information flow of 802.15.4 UWB PHY. 5

3.1 Power delay profile of CM2 CM4 CM6 and CM8. 12
3.2 Complementary Cumulative Distribution Function (CCDF) of uncaptured energy in residential environments CM1 and CM2 for n-sRAKE and sRAKE detection. 13
3.3 CCDF of uncaptured energy in office environments CM3 and CM4 for n-sRAKE and sRAKE detection. 14
3.4 CCDF of uncaptured energy in outdoor environments CM5 and CM6 for n-sRAKE and sRAKE detection. 15
3.5 CCDF of uncaptured energy in industrial environments CM7 and CM8 for n-sRAKE and sRAKE detection. 16

4.1 Simple Trellis diagram for $m = 2$. 21

5.1 BEP over LOS outdoor environment CM5 of different receivers with different number of fingers N_R. 24
5.2 BEP over NLOS residential environment CM2 of different receivers with different number of fingers N_R. 26
5.3 BEP over NLOS office environment CM4 of different receivers with different number of fingers N_R. 27
5.4 BEP over NLOS outdoor environment CM6 of different receivers with different number of fingers N_R. 28
5.5 BEP over NLOS industrial environment CM8 of different receivers with different number of fingers N_R. 29

List of Tables

2.1 Mandatory UWB PHY rate-dependent and timing-related parameters [1]. 5
2.2 Mapping of header bits, data bits and tail bits "Viterbi rate 1" [1]. . 7

Abbreviations

BEP Bit Error Probability

BPPM Burst Pulse Position Modulation

bps bits per second

BPSK Burst Position Shifting Key

CCDF Complementary Cumulative Distribution Function

CM Channel Model

CRC Cyclic Redundancy Check

DFE Decision Feedback Equalization

DS Double Side

EOD Errors Only Decoding

HSPA High Speed Packet Access

IEEE Institute of Electrical and Electronics Engineers

ISI Inter Symbol Interference

LFSR Linear Feedback Shift Register

LOS Line Of Sight

MLSE Maximum Likehood Sequence Estimator

MMSE Minimum Mean Square Error

MRC Maximum Ratio Combining

NLOS No Line Of Sight

n-sRAKE non-selective RAKE

PAN Personal Area Network

PDP Power Delay Profile

PHR Physical Header

PHY Physical layer

PRF Pulse Repetition Frequency

RS Reed Solomon

SED Successive Erasures Decoding

SHR Synchronization Header

SNR Signal to Noise Ratio

sRAKE selective RAKE

Std Standard

UWB Ultra Wide Band

WCDMA Wideband Coded Division Multiple Access

Chapter 1
Introduction

1.1 Motivation

Shannon gave a general definition to telecommunications as the transfer of information from one place to another. After some decades the idea is still the same, but the parameters getting more diverse. Multiple protocols exist in order to transfer data according to the specific needs like the type of data, transmission distance, energy restrictions, etc. The 802.15.4-2011 Ultra Wide Band (UWB) Physical layer (PHY) variant of Institute of Electrical and Electronics Engineers (IEEE) Std [1] (initially introduced as 802.15.4a) is a suitable candidate when it comes to Personal Area Network (PAN) applications and energy consumption minimization. With the above properties, 802.15.4 UWB PHY has gained great interest for contemporary and future applications to small distance communications like sensor applications. Next generation sensor networks will consist of huge number of sensors with diverse types of information, including sensors with high bit rate requirements (e.g. visual sensors). Therefore, in order to guarantee fast and successful packet transfer, a shift to higher rate modes of 802.15.4 UWB modes may be necessary.

1.2 Background

The 802.15.4-2011 UWB PHY variant of IEEE Std is able to work in various mandatory rate-dependent and time-related parameters. Following our motivation, our analysis focuses on the performance of the highest rate mandatory mode that reaches, nominally, 27.24 Mbps. This mode (mentioned as "Viterbi rate 1") includes a Reed Solomon (RS) coding scheme with a combined Burst Position Shifting Key (BPSK) Burst Pulse Position Modulation (BPPM) modulation scheme without burst spreading, in contrast to lower rate modes that include an additional inner convolutional coding scheme and spreading of the bursts. The realistic IEEE standardized channel models found in [2] are used for the detail simulation. It includes various environments i.e., residential, office, outdoor and industrial, for both Line Of Sight (LOS) and No Line Of Sight (NLOS). Some of those NLOS environments present high delay spread which makes the high rate modes rather vulnerable to multipath propagation. This is due to the fact that significant multipath components may arrive in delay spreads greater than the

specified guard interval between transmitted bursts, and may cause severe Inter Symbol Interference (ISI) between successive symbols.

1.3 Scope of thesis

To the best of our knowledge, the performance of standardized high rate 802.15.4 UWB PHY has not been analyzed before. The purpose of this thesis is to perform an evaluation of the protocol for high speed data rate, introduce Maximum Ratio Combining (MRC), MRC with ISI cancellation, MLSE & RAKE combination coherent receivers for diversity, ISI mitigation or both. Moreover, we apply optimal errors and erasures decoding in order to further improve the systems overall performance. In order to perform the evaluation we reason the choice of selective RAKE (sRAKE) from non-selective RAKE (n-sRAKE) and the choice of simulating over NLOS and not LOS. The simulation was done over realistic IEEE standardized channel models [2].

1.4 Previous work

A performance evaluation of 802.15.4 UWB PHY for the lower data rate modes (mentioned as "Viterbi rate 0"), where the systematic convolutional encoder and burst spreading is active, can be found in [3]. They derived to a semi-analytical expression for both coherent and non coherent RAKE receivers over the same Channel Model (CM) found in [2]. Research regarding pulse design can be found in [4, 5] and for modulation can be found in [6, 7, 8]. Low complexity RAKE reception techniques can be found in [9], while new receivers for generalized UWB in [10] and an analytic method to Bit Error Probability (BEP) calculation in [11]. Among others, ISI mitigation literature with combinations of MLSE and RAKE for is not rich. Specifically, a MLSE-RAKE scheme for Double Side (DS) UWB uncoded BPSK was considered in [12], [13], a Minimum Mean Square Error (MMSE) equalizer with RAKE for uncoded BPSK was analyzed in [14] and for MRC with the presence of narrow band interference in [15]. In all cases, no evidence of high bit rates in the order of tens of Mbps is given and the transmission technique is rather simplified in comparison to the standardized IEEE 802.15.4 UWB PHY. On the other hand, high rate UWB modes (non-IEEE 802.15.4) with MLSE and MRC were considered in [16] and the references therein, where simple energy detection with no channel coding was analyzed.

1.5 Methodology

In order to build the 802.15.4 UWB PHY simulator we used Matlab, where we develop both transmitter and receiver. This consists of a systematic RS encoder, BPSK and BPPM modulation and the overall process of signal creation. The implemented receivers are able to demodulate the received signal and proceed with the systematic RS decoding. We also introduced the option of optimal Successive Erasures Decoding (SED) to further decrease the BEP. The available IEEE CM

used for this simulation can be found in [2] where a Matlab code is included. We created 10000 impulse responses for each CM where we introduced into our own simulator.

1.6 Thesis outline

The rest of the thesis is organized as follows. Chapter 2 gives a description of 802.15.4 UWB PHY protocol in detail, including frame structure, information bit flow, channel coding, modulation, symbol structure and pulse shaping. In Chapter 2 we give more information regarding the CM we used and their statistical properties, while on Chapter 4 we give an analytic description of MRC, MRC with ISI cancellation and MLSE & RAKE combination receivers. In Chapter 5 we evaluate the performance of those receivers, under the channel models presented above and Chapter 6 concludes the thesis with the most important observations and future work that could be done.

Chapter 2

Description of 802.15.4 UWB PHY

This chapter provides an overall look on the frame structure and specifically the flow of the payload bits which includes coding, modulation and symbol structure. The whole chapter is divided into five sections, at the first section we analyze frame structure and the different transmission schemes, on the second section we describe the flow of the payload bits, the third section is dedicated to describe the active channel coding, the fourth section is for the bit mapping and the overall symbol structure and the fifth section is dedicated to pulse shaping.

2.1 Frame structure and mandatory transmission schemes

The frame structure of 802.15.4 UWB PHY [1] is consists of three blocks and it can be seen in Figure 2.1. The first block is Synchronization Header (SHR) Preample and it is responsible for the synchronization between transmitter and receiver. For our analysis we assume perfect synchronization which means we can ignore the existence of this block. As we will see below at Table 2.2, the next block, Physical Header (PHR) always includes the convolution encoding. This translates to a better BEP performance, thus the existence of this block can be ignored as well. Finally, the data field that contains the actual information or payload bits, has a maximum length of 127 octets or else 1016 bits. For sake of simplicity with an RS of maximum 330 input bits and output of 378 bits we define the length of one frame to be three codewords of payload bits, resulting to 1134 bits.

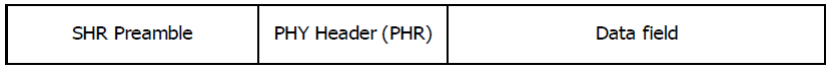

Figure 2.1: Frame structure of 802.15.4 UWB PHY [1].

In Table 2.1 we see that the IEEE 802.15.4 UWB PHY standard contains different mandatory modes with rate-dependent and timing-related parameters. The highest achievable bit rate for the mandatory channels {0:3, 5:6, 8:10, 12:14}, peak Pulse Repetition Frequency (PRF) of 499.2 MHz, bandwidth of 499.2 MHz and preamble code length of 31 is 27.24 Mbps. The specific case of 27.24 Mbps skips the systematic convolutional encoder and uses one chip per burst, meaning that the implementation of the convolution encoder and the spreading sequence is not taken into consideration in our analysis.

Table 2.1: Mandatory UWB PHY rate-dependent and timing-related parameters [1].

Modulation & Coding			Data Symbol Structure					Data		
Viterbi Rate	RS Rate	Overall FEC Rate	#Bursts Positions per Symbol N_{burst}	#Hop Bursts N_{hop}	#Chips Per Burst N_{cpb}	Burst Duration T_{burst}(ns)	Symbol Duration T_{dsym}(ns)	Symbol Rate (MHz)	Bit Rate Mbps	Mean PRF (MHz)
0.5	0.87	0.44	32	8	128	4096	256.41	0.12	0.11	15.60
0.5	0.87	0.44	32	8	16	512	32.05	0.98	0.85	15.60
0.5	0.87	0.44	32	8	2	64	4.01	7.80	6.81	15.60
1	0.87	0.87	32	8	1	32	2.00	15.60	27.24	15.60
0.5	0.87	0.44	128	32	32	4096	64.10	0.12	0.11	3.90
0.5	0.87	0.44	128	32	4	512	8.01	0.98	0.85	3.90
0.5	0.87	0.44	128	32	2	256	4.01	1.95	1.70	3.90
1	0.87	0.87	128	32	1	128	2.00	3.90	6.81	3.90

2.2 Information flow

The IEEE 802.15.4 UWB PHY signal flow is shown in Figure 2.2. It consists of five blocks starting with a systematic RS encoder (63,55) followed by a systematic convolutional encoder (with $R_s = 1/2$) where each pair of resulting bits is directed to a BPSK/BPPM modulator, forming the systems' modulation. The final discrete symbol structure is completed after applying time hopping and spreading. In order to proceed with the symbol transmission we are using the mandatory pulse shaping of root raise cosine and we have the transmitted signal $s(t)$.

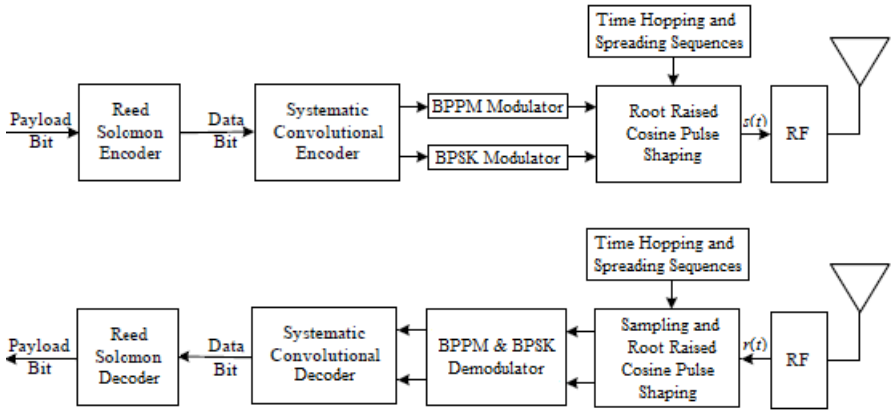

Figure 2.2: Information flow of 802.15.4 UWB PHY.

On the other side the received signal $r(t)$ is first sampled with using the root raised cosine, with perfect knowledge of time hopping and spreading we remove the time hopping and like the every spread spectrum systems, a correlator is removing the spreading. We then move on to the RAKE receiver where is implemented in order to capture the power that is dispersed by multipath into complex channel gain, know as fingers or taps. There are two types of RAKE receivers that can capture the dispersed power, first one is n-sRAKE and the second one is sRAKE. The former captures the complex gain successively from the first till a pre-defined

point, while the latter evaluates and selects the strongest. Then it is the turn of the systematic convolutional encoder to decode the demodulated bits and then the systematic RS encoder to complete the decoding and give the received payload bits.

2.3 Channel coding

The IEEE 802.15.4 UWB PHY standard implements a systematic RS encoder (63,55) followed by a systematic convolutional encoder (with $R_s = 1/2$). As mentioned above, for the high speed data rate case the systematic convolutional encoder is not implemented. For further improvement of the systems performance we introduce erasures decoding.

The systematic RS encoder belongs to the block-based error correcting codes and as block coder they have maximum distance separable between codewords. The RS (63,55) code is formed with the Galois field GF(2^6) and the generator polynomial and a primitive polynomial $p(x) = x^6 + x + 1$. The RS encoder accepts only 330 data bits and in case that a smaller number of bits are input, dummy bits are added in order to reach the 330 data bit stream. The block of 330 input bits $x_0, x_1, \ldots, x_{329}$ is properly converted to a block of 55 GF RS information symbols $X_0, X_1, \ldots, X_{54}$, each one represented as $D_i = d_{(6i+5)}, d_{(6i+4)}, \ldots, d_{6i}$ with $i = 0 \ldots 54$. The RS (63,55) encoder outputs a block of 63 encoded symbols $U_0, U_1, \ldots, U_{63}$ which are further converted to a bit sequence of 378 coded bits $u_0, u_1, \ldots, u_{377}$. In the absence of convolutional encoding and spreading the coded bits are then moved to the modulation circuit.

When the RS decoder fails to decode successfully the received codeword, the residual bit error probability is usually higher. Therefore, in order to lower the post-decoding (residual) error probability we assume that for every non decodable codeword, the decoder is aware of its failure and outputs the received RS information symbols (or the corresponding bits) unchanged. This can ideally be achieved by using a Cyclic Redundancy Check (CRC) code, which is almost always engaged in contemporary systems, including 802.15.4.

In any receiver case, the RS decoder may either engage Errors Only Decoding (EOD), that can correct up to any $t = \lfloor (d_{min} - 1)/2 \rfloor$ RS symbol errors, or errors-and-erasures decoding, where some of the received symbols are erased before decoding, according to a specific quality criterion [17]. An RS (n, k) code can correct ϵ errors and z erasures in all cases that $2\epsilon + z < d_{min}$ holds, where $d_{min} = \lfloor (n - k + 1)/2 \rfloor$. Especially in the case of the MLSE decoder, one under consideration, this criterion could be defined by taking into account the difference of the soft metrics of the possible symbols at each symbol epoch. A scheme with errors-and-erasures decoding has been also used with combined RS - convolutional coding [3].

In order to enhance performance further SED schemes can be engaged [18]. The optimum, however, most complex scheme, is to repeat decoding for every possible combination of z erasures out of n symbols, provided that $z \leq d_{min} - 1$, until decoding succeeds. This scheme, although impractical from a complexity point of view, it provides a lower bound on the errors and erasures decoding capabil-

ity. Any other errors and erasures decoding scheme will have a BEP performance between the EOD and SED.

2.4 Modulation and symbol structure

The resulting bits of the systematic RS encoder and the lack of systematic convolutional encoder are divided into two separate bit stream which they lead to BPPM or BPSK as shown in Table 2.2. The bit stream that leads to BPPM defines the transmitted burst, is named as position bit and is $b_m = u_{2m}$ while the bit stream that leads to BPSK defines the polarity of the bit on the predefined burst, is named as polarity bit and is $a_m = u_{2m+1}$, where $m = 0, \ldots, 178$ is the symbol number.

Table 2.2: Mapping of header bits, data bits and tail bits "Viterbi rate 1" [1].

Symbol #	Input Data	Position bit	Polarity Bit	
0	H_0	0	H_0	21 symbols of header at 850 kb/s
1	H_1	H_0	H_1	
2	H_2	H_1	$H_0 \oplus H_2$	
3	H_3	H_2	$H_1 \oplus H_3$	
...	...	...	...	
16	H_{16}	H_{15}	$H_{14} \oplus H_{16}$	
17	H_{17}	H_{16}	$H_{15} \oplus H_{17}$	
18	H_{18}	H_{17}	$H_{16} \oplus H_{17}$	
19	T_0	H_{18}	$H_{17} \oplus T_0$	
20	T_1	T_0	$H_{18} \oplus T_1$	
21	D_0, D_1	D_0	D_1	m symbols of data at data rate, e.g., 6.8 Mb/s
...	D_2, D_3	D_2	D_3	
...	...	...	...	
m+19	D_{m-6}, D_{m-5}	D_{m-6}	D_{m-5}	
m+20	D_{m-4}, D_{m-3}	D_{m-4}	D_{m-3}	
m+21	D_{m-2}, D_{m-1}	D_{m-2}	D_{m-6}	

The overall BPPM/BPSK is a low complexity, high performance modulation scheme while spreading and hopping offer the existence of multiple user environment. From the receiver's point of view, it offers both non-coherent and coherent reception for the cases that the convolutional encoder is active. The non-coherent receiver can detect and recover the data stream without the knowledge of the complex path gains of the channel offering a low cost option but with limited performance. On the other hand the coherent receiver with reliable knowledge of some complex path gains of the channel is a higher cost and a higher performance design. For our case where the convolutional encoder is not included, we are limited to coherent receivers, were we assume perfect knowledge of the complex path gains of the channel.

The structure of the BPSK/BPPM symbols can be seen with the timing detail in Table 2.1 for the mandatory 27.24 Mbps data rate transmission. This specific

transmission uses one chip per burst thus its implementation of the spreading sequence will not have any difference to the final BEP, although the scrambler is required for the generation of the hopping sequence $n_{h,m}$. The overall scrambler is a pseudo-random binary sequence generator with a Linear Feedback Shift Register (LFSR). The polynomial for the scrambler generator is $g(D) = 1 + D^{14} + D^{15}$ where D is a single chip delay and the corresponding scrambler output is generated by $s_n = s_{n-14} \oplus s_{n-15}$ with $n = 0, 1, 2, \ldots$. The initial state of the LFSR is determined by the preamble code and the hopping sequence is computed by $n_{h,m} = s_{kN_{cpb}} + 2s_{1+kN_{cpb}} + 4s_{2+kN_{cpb}}$.

The overall transmit signal can be written as

$$s(t) = \sqrt{E_s} \sum_{m=0}^{M-1} (1 - 2a_m) p(t - mT_s - b_m T_{BPM} - n_{h,m} T_c), \tag{2.1}$$

where, E_s is the energy per symbol, $p(t)$ is the pulse shaping waveform, T_c is the burst (and chip) duration, $T_s = N_s T_c$ is the symbol duration, $T_{BPM} = N_{BPM} T_c$ is the BPM interval that is equal to half of the symbol period (i.e., $N_s = 2N_{BPM}$), and is divided into two equal parts, that is, the transmission period and the guard period. Each transmission period consists of N_{hop} burst positions and $n_{h,m}$ is the time hopping sequence that determines the burst position to be used within the BPM interval, taking values in $0, \ldots, N_{hop} - 1$. The values of the parameters can be found in Table 2.1 above.

2.5 Pulse shaping

The 802.15.4 UWB PHY have the capability of transmitting several optional pulses. The beacon frames although shall always be transmitted with the use of mandatory pulse shaping and all other frames may be transmitted with an optional pulse if both receiver and transmitter are capable of supporting it. The constrain of the transmitted pulse shape $p(t)$ is the cross-correlation function of a standard reference pulse $r(t)$. The normalized cross-correlation between the two waveforms is,

$$\phi(\tau) = \frac{1}{\sqrt{E_r E_p}} \mathrm{Re} \int_{-\infty}^{\infty} r(t) p^*(t + \tau) dt$$

where E_r and E_p are the energies of $r(t)$ and $p(t)$ respectively. The reference pulse $r(t)$ is a root raised cosine pulse and takes shape of,

$$r(t) = \frac{4\beta}{\pi\sqrt{T_p}} \frac{\cos[(1+\beta)\pi t/T_p] + \frac{\sin[(1-\beta)\pi t/T_p]}{4\beta(t/T_p)}}{1 - (4\beta t/T_p)^2},$$

where the roll-off factor of the root raised cosine pulse is $\beta = 0.5$ and T_p is the inverse of the chip frequency and for our case $T_p = 2$ ns. A standard compliant UWB PHY transmitter shall have a pulse $p(t)$ with magnitude of cross correlation $|\phi(\tau)|$ greater or equal to 0.8 for at least $T_w = 0.5$ ns. For any side lobes the magnitude of cross correlation $|\phi(\tau)|$ shall be no grater than 0.3.

A variety of pulse shapes can be found in [19], where the authors purpose various pulses. Some of them are the Rectangular monocycle, the Rayleigh monocycle, the Laplacian monocycle, the Cubic monocycle and a large category of Gaussian pulses. The family of the Gaussian pulses are derived from the simple monocycle and its higher-order derivatives. These higher-order derivatives are generated by the successive filtering of the Gaussian pulse. A more detailed analysis of the pulse shaping can be found in [20] where they generate multiple orthogonal pulses that can be utilized for higher data rate or lower error rate. In [5] the authors proposed a different chirp pulse based UWB system that improves energy consumption and the overall complexity is current CMOS technology. The propose receiver achieves significantly better performance with the same computational complexity but with a high complexity transmitted waveform.

Although the extensive study in the current literature, for our analysis the pulse shaping, match filtering and synchronization is considered to be optimal. This means we do not apply any gain or loss of dB in the Signal to Noise Ratio (SNR) scale.

Chapter 3
Channel Models

This chapter provides a summary of the UWB channel models used to simulate the IEEE 802.15.4 UWB PHY system including different environments and their channel properties. The whole chapter is divided into two sections. In the first section we present the available environments and present the way we create the UWB CM, while in the second section we provide an analysis of the channel statistics and predict how they will effect the simulation.

3.1 IEEE Channel Models

UWB channel models are fundamentally different from the narrow band ones but their modeling with statistical parameters remains the same. For our simulation we use the 802.15.4 channel model found in [2] where it contains a Matlab code able to output impulse responses for 9 different environments and cases. The environments are residential LOS and NLOS (CM1 CM2), office LOS and NLOS (CM3 CM4), outdoor LOS and NLOS (CM5 CM6), industrial LOS and NLOS (CM7 CM8) and Outdoor farm LOS (CM9). For the analysis we are solely take account all the NLOS cases for each environment CM2, CM4, CM6, CM8, reasoning that this is the worst case scenario thus the harder to resolve.

The analysis and simulation takes into account only small scale fading with an extension of modifying the averages signal to noise ratio depending on the distance between transmitter and receiver. The channel models follow a modified Saleh-Valenzuela model with arrival of paths (rays) in clusters, mixed Poisson distribution for ray arrival times and possible delay dependence of cluster decay time. Small scale fading amplitude statistics follow a Nakagami distribution with different m factors for different components and block fading, where the channel stays constant over data burst duration. The simulation assumes block fading, where the channel stays constant over a transmission frame, an assumption validated by large coherence times in slowly-changing indoor environments. These models only treats the channel but with the existence of antenna measurements, antenna effects can be modeled and added separately, something that was not implemented in our basic simulation. The impulse response $h(t)$ consists of L_c clusters of L_r

rays and can be expressed (in complex baseband) as

$$h(t) = \sum_{l=0}^{L_c-1} \sum_{k=0}^{L_r-1} \beta_{k,l} e^{j\phi_{k,l}} \delta(t - T_l - \tau_{k,l}) \tag{3.1}$$

where, $\delta(t)$ denotes the Dirac delta function, $\beta_{k,l}$ is the amplitude of the kth component in the lth cluster, T_l is the delay of the lth cluster, $\tau_{k,l}$ is the delay of the kth multipath component relative to the lth cluster arrival time T_l, and $\phi_{\kappa,\lambda}$ is uniformly distributed in $[0, 2\pi)$. The statistics of the path gains and delays above mentioned can be found in [2] for different channel models (CMs). To simplify the notation we use, in the following, the equivalent model

$$h'(t) = \sum_{\lambda=0}^{\Lambda-1} g_\lambda \delta(t - \tau_\lambda) \tag{3.2}$$

where, $\Lambda = L_c L_r$ is equal to the number of all rays of all clusters, g_λ is the complex path gain of the λth ray, and τ_λ is the corresponding delay. We assume that the channel path gains are normalized so that $\sum_{\lambda=0}^{\Lambda-1} E[g_\lambda^2] = 1$.

3.2 Channel statistics

This section is divided into two subsections. In the first subsection we provide the Power Delay Profile (PDP) for the available CMs for both LOS and NLOS, while in the second subsection we provide the CCDF for the available CMs for both n-sRAKE, sRAKE with a low and high number of fingers.

3.2.1 Power Delay Profile

The main factor affecting the performance of the highest data rate mode is the ISI arising from delayed multipath components. The delay spreads for every simulating channel model can be seen in Figure 3.1 taken from 10000 channel realizations. The high data rate BPM has a duration of 32 ns and each symbol is 2 BPM the overall symbol duration is 62 ns. Any significant interfering multipath components around -10 dB that extend over 32 ns can cause intraburst interference and if they extend over 62 ns they cause ISI.

More specifically for the LOS only outdoor environment CM5 with a delay of 60 ns with average power of -12 dB might have some ISI and intraburst interference. The residential environment CM1 with a delay of 30 ns and average power of -10 dB might only appear intraburst interference.

For the LOS environments the intraburst interference should be taken as granted. The only environment that avoids ISI is office CM4, since for a delay of 60 ns the average power is down to -14 dB. On the other hand, industrial CM8 for a delay of 60 ns the average power is -10 dB and residential CM2 for the same delay the average power is -6 dB. That means that both environment will appear to have some ISI and for the residential CM2 it is going to be even bigger. The worse case of all is the outdoor CM6, since in order to drop at the average power of -10 dB the delay goes up to 330 ns. That results to a heavy ISI environment where multiple past symbols will stack making ISI mitigation receiver a requirement.

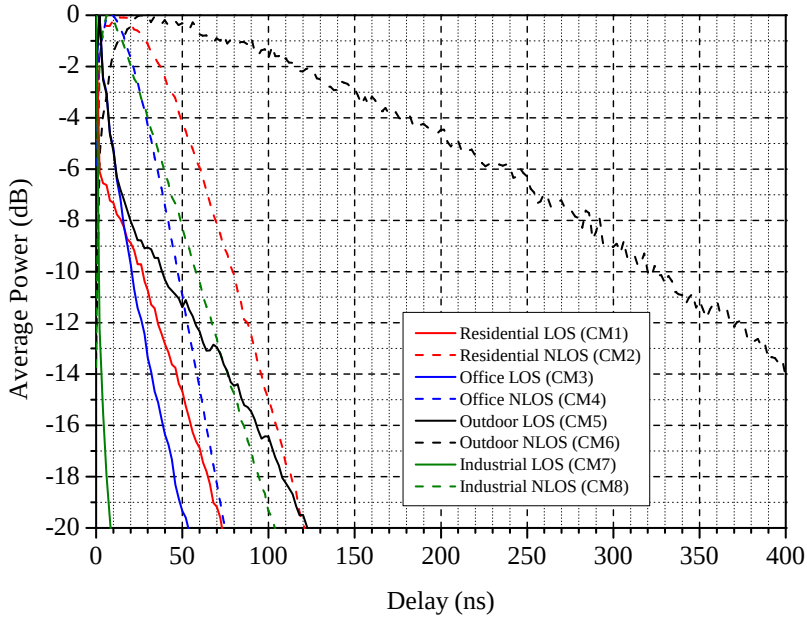

Figure 3.1: Power delay profile of CM2 CM4 CM6 and CM8.

3.2.2 CCDF of RAKE uncaptured energy

In this subsection we are going to look at the CCDF of the uncapture energy for each environment. Each sub-subsection is dedicated to the corresponding environment for both LOS, NLOS cases and a n-sRAKE, sRAKE receivers. The reason to include this metric is to give a general idea regarding the percentage of energy the two RAKE schemes are missing to capture at the different CMs.

Residential Environments CM1 CM2

For the residential environment and Figure 3.2 we can see that for NLOS the n-sRAKE has 0.3 probability to uncapture 10% of the energy, while the sRAKE only has 0.06 probability to uncapture 10% of the energy. The difference between n-sRAKE and s-RAKE is substantial where the s-RAKE is expected to outperform the n-sRAKE.

For the LOS case the difference between them is much smaller. For the n-sRAKE the probability to uncapture the 10% of the energy is down to 0.1 while for the s-RAKE is 0. This means we should expect a small difference in their performance. Overall the NLOS sRAKE seems capable to capture a good percentage of overall energy and will not have issues in performance regarding the energy dispersion.

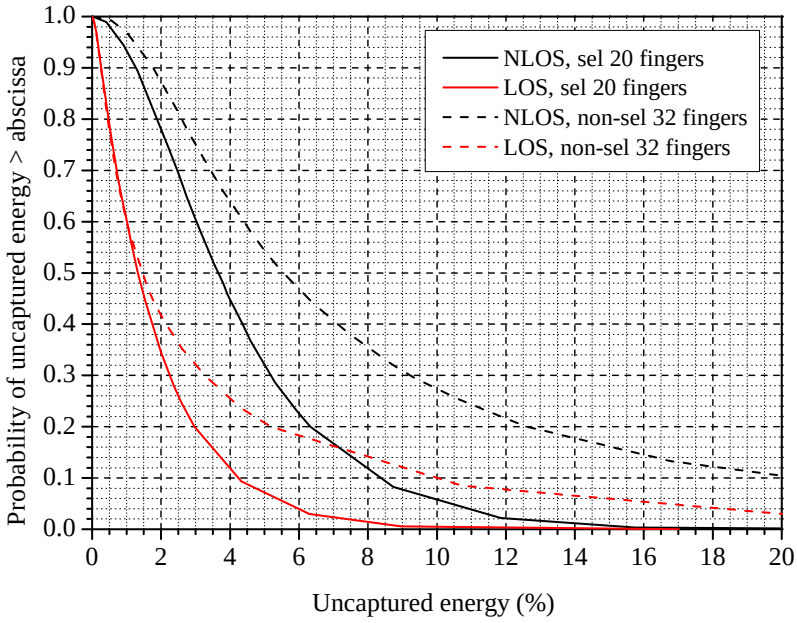

Figure 3.2: CCDF of uncaptured energy in residential environments CM1 and CM2 for n-sRAKE and sRAKE detection.

Office Environments CM3 CM4

For the office environment, as depicted Figure 3.3 we can see that for NLOS the n-sRAKE has 0.02 probability to uncapture 5% of the energy and 0 probability to uncapture 10% of the energy. Meanwhile the sRAKE has 0.36 probability to uncapture 5% of the energy and 0.6 probability to uncapture 10% of the energy. Even though the 0.36 probability to uncapture 5% of the energy seems high, the 5% is considered to be a small percentage, thus it will not have significant change in the overall performance.

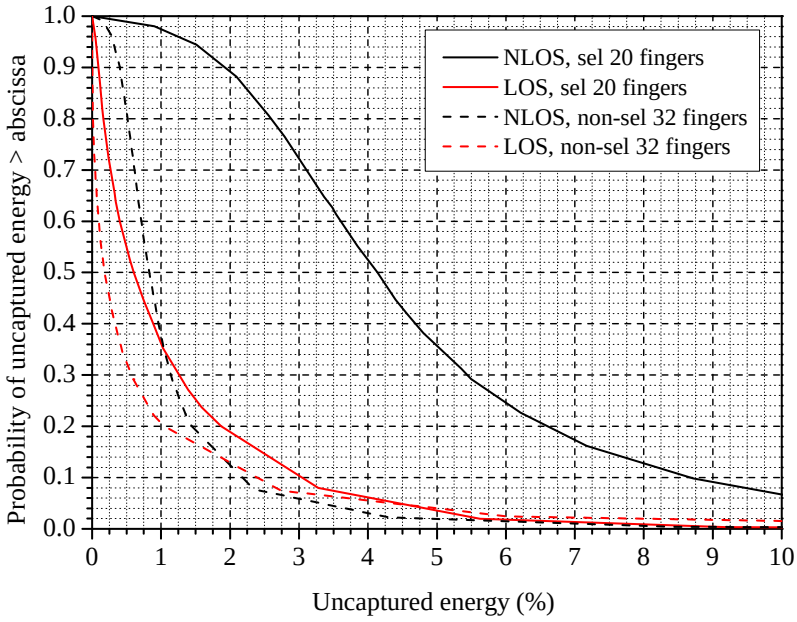

Figure 3.3: CCDF of uncaptured energy in office environments CM3 and CM4 for n-sRAKE and sRAKE detection.

For the LOS case the difference is extremely small, even for small percentages like 1% or 2%. Going back to Figure 3.1 we can see the office has the best performance for the NLOS case. That explains the fact that the n-sRAKE is able to collect more energy than the sRAKE.

Outdoor Environments CM5 CM6

The outdoor environment in Figure 3.4 is the most interesting environment. For the NLOS case and a 20% uncaptured energy the sRAKE is at 0.48 probability, while it is up to 0.94 for the n-sRAKE. This means that both n-sRAKE and sRAKE are going to miss a huge percentage of the energy, but only the n-sRAKE is probably unable to attain an acceptable BEP. Moreover when the sRAKE has 0

probability to uncapture the 40% of the energy, the n-sRAKE has 0.8 probability. By any means the n-sRAKE is unable to perform in the outdoor NLOS CM6 environment.

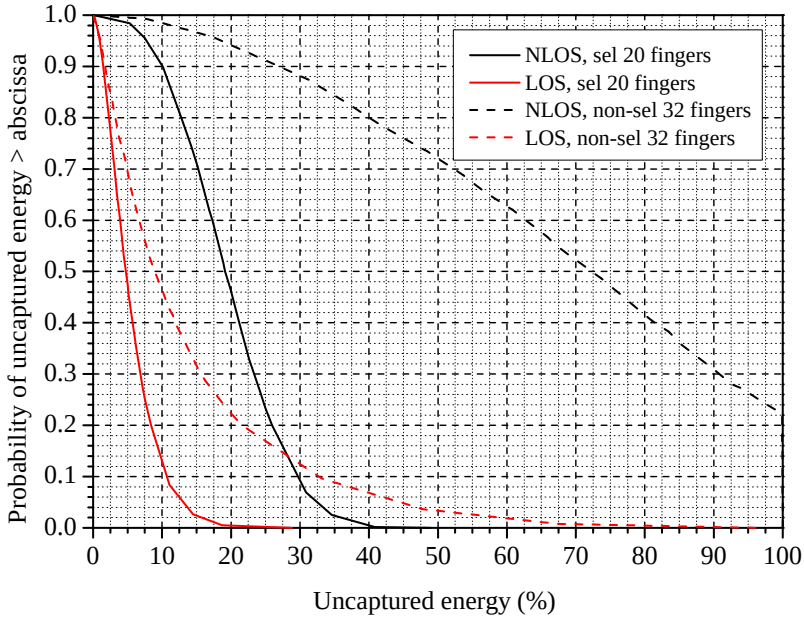

Figure 3.4: CCDF of uncaptured energy in outdoor environments CM5 and CM6 for n-sRAKE and sRAKE detection.

For the LOS cases, the probability to uncapture 10% of the energy for the sRAKE is at 0.1 while for the n-sRAKE it is up to 0.48. We can see that even for the LOS case the n-sRAKE has high probability to uncapture a large percentage of energy. Another example, while for sRAKE the probability to uncapture 20% of the energy is 0, for the n-sRAKE it is up to 0.22.

In comparison with the PDP in Figure 3.1 we can understand why sRAKE is able to capture more energy than the n-sRAKE. The starting of curve of CM6 implies that the starting fingers are going to have less energy than the delayed fingers. That means a n-sRAKE is unable to include the fingers that contain the actual power.

Industrial Environments CM7 CM8

For the industrial environment and Figure 3.5 in the NLOS case we can see that the probability to uncapture 10% of the energy for the n-sRAKE is 0.02 while for the sRAKE it is at 0.4. The difference might seem significant but the percentage is small, thus the sRAKE will not have any issues regarding performance. We can

see that with the probability to uncapture the 15% of the energy is 0 for n-sRAKE but this time for the sRAKE is down to 0.01.

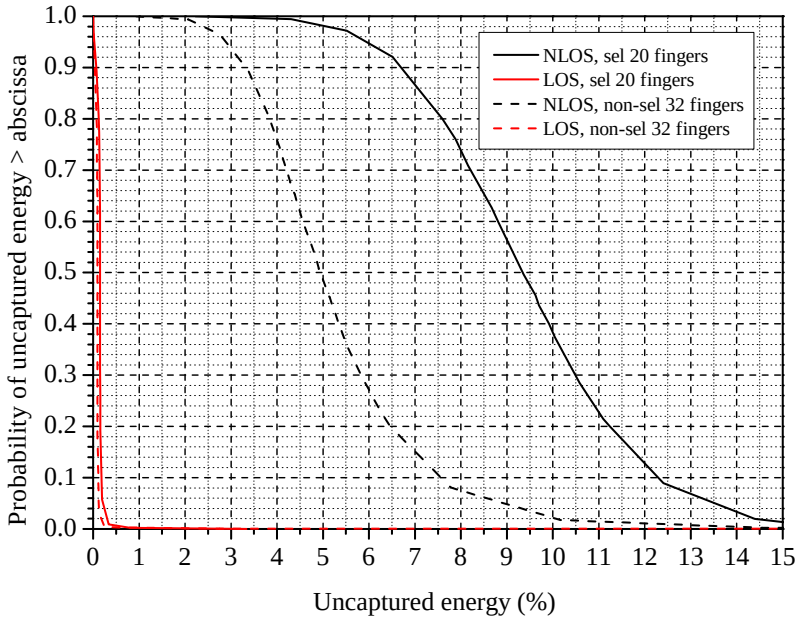

Figure 3.5: CCDF of uncaptured energy in industrial environments CM7 and CM8 for n-sRAKE and sRAKE detection.

Regarding the LOS case, there is not much analysis to be done. As expected from the PDP in Figure 3.1 CM7 has the shortest delay spread, thus not much of energy will left uncaptured.

Chapter 4
Receivers

This chapter provides a description of the received signal, different RAKE applications and various coherent receivers are simulated with or without the ability to mitigate the ISI. The whole chapter is divided into four sections, on the first section we analyze the received signal and the reason that sRAKE receiver is important, on the second section we explain the MRC receiver, on the third section we expand the MRC receiver with ISI cancellation and on the fourth section we present and reason the MLSE & RAKE combination receiver.

4.1 Received signal and reasoning of RAKE implementation

In order to formulate the received signal mathematically we assume perfect synchronization, match filtering and we also ignore the path loss. The received signal can be expressed as,

$$r(t) = \sqrt{E_s} \sum_{m=0}^{M-1} \sum_{\lambda=0}^{\Lambda-1} g_\lambda (1-2a_m) p(t - mT_s - b_m T_{BPM} - n_{h,m} T_c - \tau_\lambda) + n(t), \quad (4.1)$$

where, $n(t)$ represents the additive white Gaussian noise process. Assuming perfect sampling per chip interval, the discrete-time version of the received sampled signal may be presented as,

$$r[n] = \sum_{m=0}^{M-1} \sum_{\lambda=0}^{\Lambda-1} g_\lambda (1-2a_m) \delta[n - mN_s - b_m N_{BPM} - n_{h,m} - n_\lambda] + \nu_n, \quad (4.2)$$

where we have assumed, without loss of generality, that the path delays are multiples of the chip duration, that is $\tau_\lambda = n_\lambda T_c$. Additionally, $\delta[\cdot]$ represents the Kronecker delta function and ν_n is the complex Gaussian noise sample of variance N_0/E_s (the signal energy is embodied in the noise variance for notation simplicity).

For any receiver, the sequence numbers of the samples corresponding to the lth path of the mth symbol may be expressed as,

$$\mu_{m,\lambda}^{(b_m)} = mN_s + b_m N_{BPM} + n_{h,m} + n_\lambda, \quad (4.3)$$

and can be further split to one sample per BPM interval for the l path of the mth symbol as,

$$\begin{aligned}\mu_{m,\lambda}^{(0)} &= mN_s + n_{h,m} + n_\lambda \\ \mu_{m,\lambda}^{(1)} &= mN_s + N_{BPM} + n_{h,m} + n_\lambda\end{aligned} \tag{4.4}$$

for $b_m = 0$, and $b_m = 1$, respectively.

The sample with sequence number given by (4.3) includes, in addition to the useful signal of the lth path of the mth symbol, ISI terms from the previous symbols. In particular, the pth previous symbol's path λ_p that will add up to this sample is the one with delay equal to

$$n_{\lambda_p} = \mu_{m,\lambda}^{(b_m)} - (m-p)N_s - b_{m-p}N_{BPM} - n_{h,m-p}, \tag{4.5}$$

whenever $n_{\lambda_p} \leq n_{\Lambda-1}$. Therefore, the total ISI interfering with the lth path of the mth symbol can be expressed as,

$$I[\mu_{m,\lambda}^{(b_m)}] = \sum_{p=1}^{P} g_{\lambda_p}(1 - 2a_{m-p}), \tag{4.6}$$

where, λ_p is the interfering path with delay given by (4.3), and P, the total number of previous symbols producing ISI to the current symbol, depends on the delay spread of the channel.

The RAKE receiver is employed in order to gather some of the transmitted symbol energy that it is been dispersed by multipath, by combining coherently Λ_r paths (or fingers). The way of selecting the Λ_r fingers has been studied extensively in the past in [3].

As mentioned earlier, we analyze two options of RAKE implementation, the n-sRAKE that we successively take the fingers from the first until a certain predefined point and the sRAKE that evaluates the power of each finger and selects those that offer the highest absolute gain. The n-sRAKE has the disadvantage of selecting multiple paths where the actual signal power is low compared to the noise and ISI power, resulting to working with more interference and noise than actual signal power. On the other hand, the n-sRAKE does not need to evaluate the complex channel gains thus avoiding some complexity. For the second situation of sRAKE we evaluate and select the fingers that are expected to have more signal power. In this situation we add some overall complexity with the ability to receiver more signal power and less ISI power. Comparing the two situations the sRAKE is by far the best choice since in comparison with the n-sRAKE it requires less fingers, thus a lower number of correlators in order to gather the same amount of power.

4.2 MRC RAKE receiver

In order to introduce the maximum diversity we assume that the channel parameters are correctly estimated. These are, the time of arrival for each path, the amplitude and the phase of the signal. The MRC receiver achieves the best performance by multiplying each received sample with the corresponding conjugate

complex channel gain. The result is the compensation of the phase shift and the weighting of each finger with a factor that is proportional to the signal strength.

The Λ_R samples with sequence numbers given by (4.4) are properly weighted and added to derive the decision variables

$$V^{(b_m)} = \sum_{\lambda=0}^{\Lambda_R-1} \Re\left\{ g_\lambda^* r[\mu_{m,\lambda}^{(b_m)}] \right\}. \tag{4.7}$$

The Λ_R samples are the actual RAKE fingers where in case of n-sRAKE are the successive complex path gains from the start, up until a predefined point and for the sRAKE are the complex path gains with the highest power.

The position bits are estimated by the BPM that includes the burst/chip value with the highest absolute value of the decision variables, while the sign of the decision variable determines the polarity bits, i.e.,

$$b_m = \begin{cases} 0, & |V^{(0)}| > |V^{(1)}| \\ 1, & |V^{(1)}| > |V^{(0)}| \end{cases} \tag{4.8}$$

and

$$a_m = \begin{cases} 0, & b_m \max\left(V^{(b_m)}\right) > 0 \\ 1, & b_m \max\left(V^{(b_m)}\right) < 0. \end{cases} \tag{4.9}$$

4.3 MRC ISI cancellation receiver

The MRC ISI cancellation receiver exploits the diversity introduced to the MRC receiver and attempts to mitigate the ISI that is been created by the previous symbol. For the first symbol, the MRC makes a decision regarding the transmitted symbol using the eq. (4.2). Taken as granted that the decision is correct, for the second symbol it subtracts estimated received interference eq. (4.6) of the previous transmitted symbol from the current received sample, getting the equation,

$$r'[\mu_{m,\lambda}^{(b_m)}] = g_\lambda(1 - 2a_m) - \hat{I}[\mu_{m,\lambda}^{(b_m)}]. \tag{4.10}$$

where $\hat{I}$ is the estimation of (4.6). The interfering samples are,

$$n_{\lambda_p} = \mu_{m,\lambda}^{(b_m)} - (m-p)N_s - \hat{b}_{m-p}N_{BPM} - n_{h,m-p}, \tag{4.11}$$

where $\hat{a}_{m-p}$ and $\hat{b}_{m-p}$ correspond to the estimated bits of the pth previous symbol which gives $\hat{I}[\mu_{m,\lambda}^{(b_m)}]$ the form of,

$$\hat{I}[\mu_{m,\lambda}^{(b_m)}] = \sum_{p=1}^{P_r} g_{\lambda_p}(1 - 2\hat{a}_{m-p}) \tag{4.12}$$

with P_r to be the predefined past symbols the receiver is going to take into consideration to remove.

After the part of removing the ISI is completed we then take the modified received signal and continue with the same process as the MRC receiver. We

weigh and add the altered samples to derive the new decision variables like eq. (4.7) and then decide regarding the position and polarity bits with eq (4.8) and (4.9).

For each new symbol we can subtract as many past symbols we want. The problem with this receiver is the error propagation; in case a symbol is chosen falsely we are going to remove the wrong complex channel values making it harder to derive a correct decision for the current symbol. Complexity wise the MRC ISI cancellation receiver takes advantage of the diversity of the MRC and with a small addition to complexity tries to mitigate the ISI.

4.4 MLSE & RAKE combination receiver

Maximum Likehood is the optimum way to mitigate interference when it comes to Sequence Estimators. We deploy MLSE & RAKE receiver in order to compare it with the other receivers and conclude if it is worth to compose a more complex ISI mitigating receiver in order to get some gain in the overall BEP. A basic example on how MLSE works can be found in [21].

It all starts from the first received sample, where we start building the Trellis tree diagram. The MLSE takes the received sample and calculates the Eucledian distance for each possible symbol transmission. This creates four metrics known as Eucledean distances expressed with the symbol d. After that the receiver moves on to the next received sample, where again run through all four possible transmitted symbols, only this time the estimated received symbol is the addition of the current possible symbol and the previously transmitted symbol. With this implementation the sequence estimator has an estimate of the previous symbol with a corresponding weight d, thus the estimated previous symbol is considered to cause ISI in the current symbol and the complex channel gain values can be used in order to get a better Eucledian distance. Overall each estimated received symbol will grow four more branches with the following possible transmitted symbol. The whole process up until $m = 2$ takes the shape of a Trellis tree diagram, like in Figure 4.1.

In this point it is important to stress out the complexity issue of the MLSE. As we can see in Figure 4.1 at the trellis tree diagram with m transmitted symbols the full expansion of the tree will result to 4^m sequences. The calculation of those 4^m sequences requires great computing power, if not impossible with today's technology, thus the implementation of simpler algorithm is required. With the "delete δ branches" algorithm after each estimated transmitted symbol we sum the overall Eucledean distances of each sequence and we delete the most improbable (highest value). It is important though to have a significant number of saved states in order to prevent and fix propagating errors. After extensive simulations we found out that there is an insignificant difference between $\delta = 4$ and 16 surviving sequences, thus for the purpose of our work we only simulated with $\delta = 4$ surviving sequences for each symbol.

The sRAKE or n-sRAKE receiver are applied with the selection of multiple received samples and their calculation of their corresponding Eucledean distance from the estimated received sample. Then we proceed with the summation of each

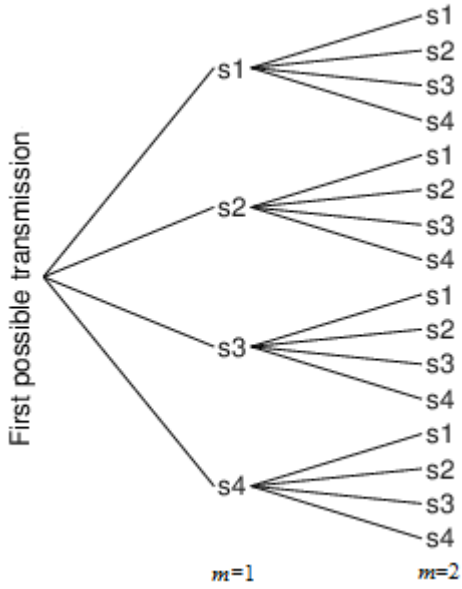

Figure 4.1: Simple Trellis diagram for $m = 2$.

finger, resulting to one value d for each symbol. Moreover, each finger is weighed according to their corresponding strength, meaning that the transmitted power on the finger effects the Eucledean distance and overall the final sequence selection.

From the above analytic description the estimated received signal is as a the addition of the received samples (4.2) and estimated received interference (4.12), it can be expressed mathematically as,

$$\hat{r}[\mu_{m,\lambda}^{(b_m)}] = g_\lambda(1 - 2a_m) + \hat{I}, \tag{4.13}$$

where, the MLSE algorithm first estimates the sample for the bth BPM of the λth path of the mth symbol and then adds the ISI caused by p symbols.

Then, it forms the Eucledean distance of the received pair of samples per symbol (one per BPM) with the corresponding estimates of the jth ($j = 1, \ldots, 4$) possible symbol that arises from the combination of all possible a_m and b_m, as described in Section 4.2, i.e.,

$$d_{m,\lambda}^{(j)} = \sqrt{\left| r[\mu_{m,\lambda}^{(0)}] - \hat{r}[\mu_{m,\lambda}^{(0)}] \right|^2 + \left| r[\mu_{m,\lambda}^{(1)}] - \hat{r}[\mu_{m,\lambda}^{(1)}] \right|^2} \tag{4.14}$$

The final metric per symbol accumulates all the RAKE fingers to produce

$$d_m^{(j)} = \sum_{\lambda=0}^{\Lambda_R - 1} d_{m,\lambda}^{(j)}. \tag{4.15}$$

Based on these metrics the algorithm estimates the most probable symbol sequence

of length M (the one presenting the minimum distance with the received symbol sequence) throughout the packet length.

Chapter 5
Results

This chapter provides results of simulations of the proposed receivers under the IEEE CMs. In all cases, 10000 channel realizations and an adequate number of packets are simulated in order to achieve convergence of the presented BEP values. In first Section we take a look into the benefits of the sRAKE with Λ_R fingers versus a n-sRAKE receiver as described in Section 4.1 and reason with the selection of simulating over NLOS environments. While on the second section we evaluate the performance of every NLOS environment with every receiver with either EOD or SED as described in Section 2.3.

5.1 Reasoning of sRAKE and NLOS

In order to show that sRAKE is a better choice over n-sRAKE and that the NLOS environments are harder to perform well we chose to simulate over outdoor LOS CM5 case with all the receivers, MRC, MRC with ISI cancellation and MLSE & RAKE combination receiver. We chose outdoor LOS CM5 because it presents the worse PDP as seen in Section 3.2 from all the LOS environments. The choice of any other LOS environment will present better results in the BEP performance.

The BEP performance of the outdoor LOS CM5 can be found in Figure 5.1. The first thing that is noticeable is the error floor in the n-sRAKE of the MRC and MRC with ISI cancellation. The n-sRAKE collects the energy successively from the first finger up to 16 or 32 leading to result of receiving more ISI than actual symbol energy. More specifically in the case of 16 fingers the received energy is so low that the BEP performance is unacceptable in a realistic system. In the case of 32 fingers the BEP drops at 10^{-4} at 18 dB for the MRC receiver, while for the MRC with ISI cancellation at 12 dB. The MRC receiver manages to achieve an acceptable BEP at a very high SNR meaning that the actual implementation can be considered unrealistic. On the other hand the MRC with ISI cancellation can be considered realistic but compared with the MLSE & RAKE the difference is around 7 dB, which is large.

If we take a look into the sRAKE case we can see that all the receivers are performing equally. Especially with the alteration in the number of fingers we can see that there is no substantial gain. That means for the worse PDP wise, LOS environment there is no big point to increase the number of fingers. That means for every other LOS environment the gain will be even smaller, thus there is no

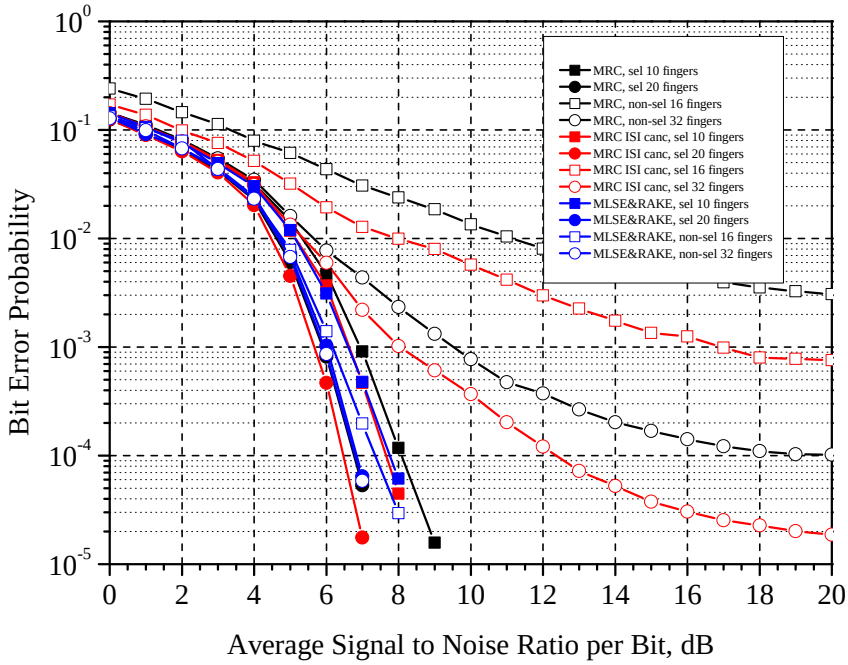

Figure 5.1: BEP over LOS outdoor environment CM5 of different receivers with different number of fingers N_R.

point of taking them into consideration.

Comparing the four MLSE & RAKE combination receivers we can see that non of them appears to have an error floor. That proves that the MLSE & RAKE combination is an optimal way to mitigate interference. In fact the n-sRAKE with a low or high number of fingers is always performing better than the corresponding sRAKE.

5.2 Performance Evaluation under IEEE CM

This section is divided into four subsections. Each subsection is devoted to a corresponding environment, first subsection for residential, second subsection for office, third subsection for outdoor and fourth for industrial. Each figure illustrates the BEP of MRC, MRC with ISI cancellation and MLSE & RAKE combination receivers versus the signal-to-noise ratio per bit E_b/N_0[1] where each case the receiver uses $\Lambda_R = 10$ or $\Lambda_R = 20$ fingers are used to combined coherently.

5.2.1 Residential environment CM2

For the residential environment and Figure 5.2 EOD cases, the MRC and MRC with ISI cancellation receivers, the increment from $\Lambda_R = 10$ to $\Lambda_R = 20$ offers 1dB gain for a BEP in the order of 10^{-4}. While for the MLSE & RAKE combination receiver attains a gain of 0.5 dB for the same order of BEP. Although for the case of $\Lambda_R = 10$ the MLSE & RAKE combination seems to perform better than the other, that does not seem to happen when $\Lambda_R = 20$. With 10 fingers the effective energy collected is not enough to utilize the MRC diversity, thus leading to wrong results, leading to an error mitigation to the MRC with ISI cancellation receiver. When the fingers increase the MRC is able to perform better thus the further improvement of the MRC with ISI cancellation.

For the SED cases and a BEP in the order of 10^{-4} the gain attained for every receiver is at 1 dB. Overall with the addition of optimal erasures the receiver is able to further increase the BEP, which translates to a more secure MRC decisions resulting to the fact that MRC ISI cancellation outperforms any other receiver.

5.2.2 Office environment CM4

For the office environment and Figure 5.3 EOD cases, the MRC receiver, the increment from $\Lambda_R = 10$ to $\Lambda_R = 20$ offers 1.5dB gain for a BEP in the order of 10^{-4}. While the MRC with ISI cancellation and MLSE & RAKE combination receivers attain a gain of 1dB for the same order of BEP. As seen in Section 3.2 BLOS office environment CM4 has the lowest delay spread of all the NLOS environments. That explains the fact that for $\Lambda_R = 10$ the MRC is 0.5dB worse than MRC with ISI cancellation and MLSE & RAKE combination. For $\Lambda_R = 20$ the

[1] The signal to noise ratio per bit equals $E_b/N_0 = \frac{1}{2}E_s/N_0$ where E_s is the transmitted energy per symbol. This assumption is valid for comparison purposes since no distance dependent path loss is considered, and the channel path gains are properly normalized to give a total (sum) power of unity.

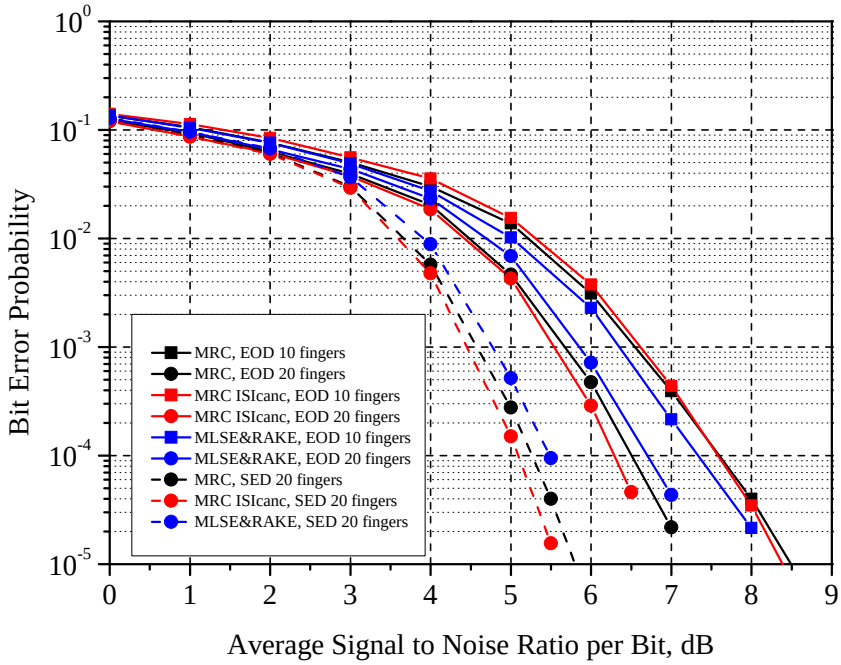

Figure 5.2: BEP over NLOS residential environment CM2 of different receivers with different number of fingers N_R.

MRC gathers higher energy and the diversity of the MRC manages to catch up with the MLSE & RAKE combination.

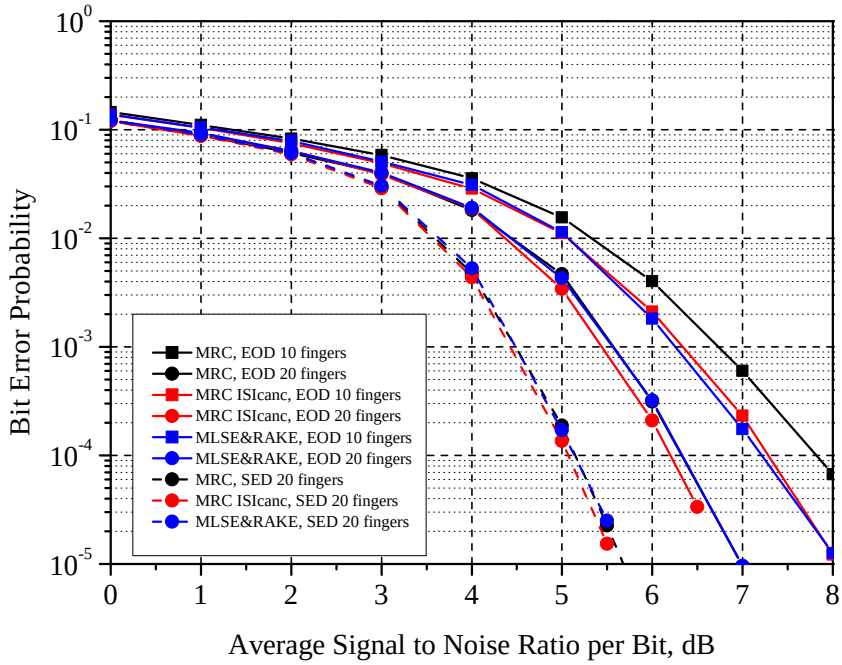

Figure 5.3: BEP over NLOS office environment CM4 of different receivers with different number of fingers N_R.

Again the SED cases and a BEP in the order of 10^{-4}, the gain attained for every receiver is at 1 dB. The low delays spread that this environment offers manages to make all the receivers perform likely. We can notice the the MRC with ISI cancellation performs slightly better due to the fact that some small ISI is mitigated but the gain is so small that it is considered to be irrelevant.

5.2.3 Outdoor environment CM6

The outdoor environment and Figure 5.4 is interesting because of its high delay profile, as seen in Section 3.2. First of all the increment of $\Lambda_R = 10$ to $\Lambda_R = 20$ for a BEP in the order of 10^{-4} offers 2 dB gain to most receivers, but MLSE & RAKE combination where the removal of two previous symbols has a gain of 1.5 dB. Specifically for the case of $\Lambda_R = 10$ the gain between the MLSE & RAKE combination with the removal of 2 past symbols and the MRC is at 1.5 dB. In comparison with the MRC with ISI cancellation is at 1 dB and between the MLSE & RAKE combination with the removal of 1 symbol is at 0.5 dB. It seems that when the received energy is low and the delay spread of the environment

is high, the ISI mitigation is extremely important. In comparison with the case of $\Lambda_R = 20$ where the received energy is higher and the ISI mitigation stays the same, the overall BEP gain is reduced. The MLSE & RAKE combination with the removal of 2 symbol has a gain of 0.5 dB over MRC, and only 0.25 dB over MRC with ISI cancellation and MLSE & RAKE combination with the removal of 1 symbol.

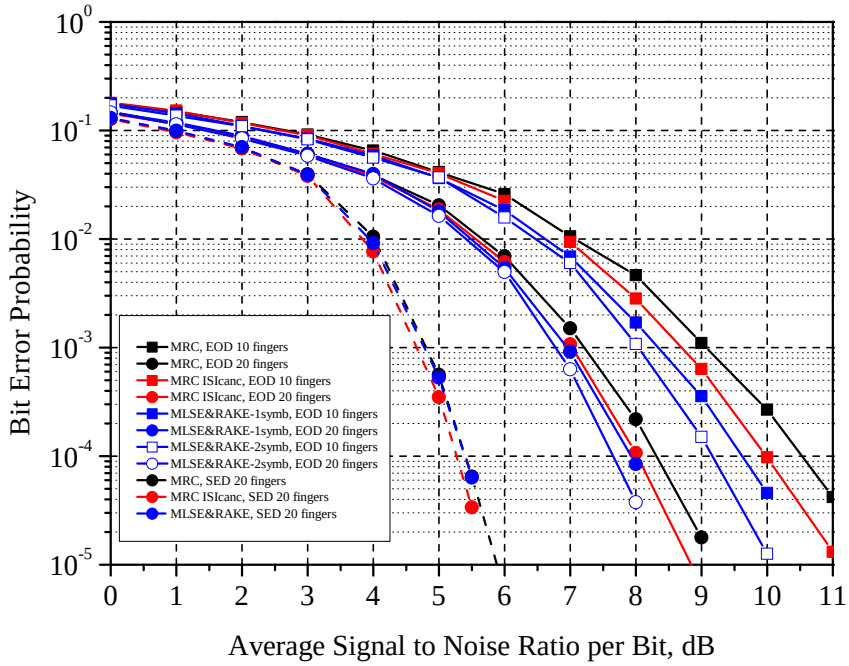

Figure 5.4: BEP over NLOS outdoor environment CM6 of different receivers with different number of fingers N_R.

For the SED cases and a BEP in the order of 10^{-4} the gain attained for the MRC is at 2.5 dB. For the MRC with ISI cancellation and MLSE & RAKE combination receivers the gain is around 2 dB. Overall it seems that the addition of the optimum SED manages to bring every receiver at the same magnitude of BEP.

5.2.4 Industrial environment CM8

For the industrial environment and Figure 5.5 EOD cases, the MRC receiver, the increment from $\Lambda_R = 10$ to $\Lambda_R = 20$ offers 1 dB gain for a BEP in the order of 10^{-4}. While for the MRC with ISI cancellation receiver the gain is at 1 dB and for the MLSE & RAKE combination receiver the gain is at 0.75 dB. The overall gain seems to drop since the energy harvest of the MRC improves the diversity and the

ISI mitigation is less needed. Only for the cases of $\Lambda_R = 10$ where the harvested energy is lower, the MLSE & RAKE combination receiver has a gain of 0.5 dB and 0.25 dB over the MRC and MRC with ISI cancellation receivers. When the energy is higher, at $\Lambda_R = 20$ all the receivers seem to have the same BEP.

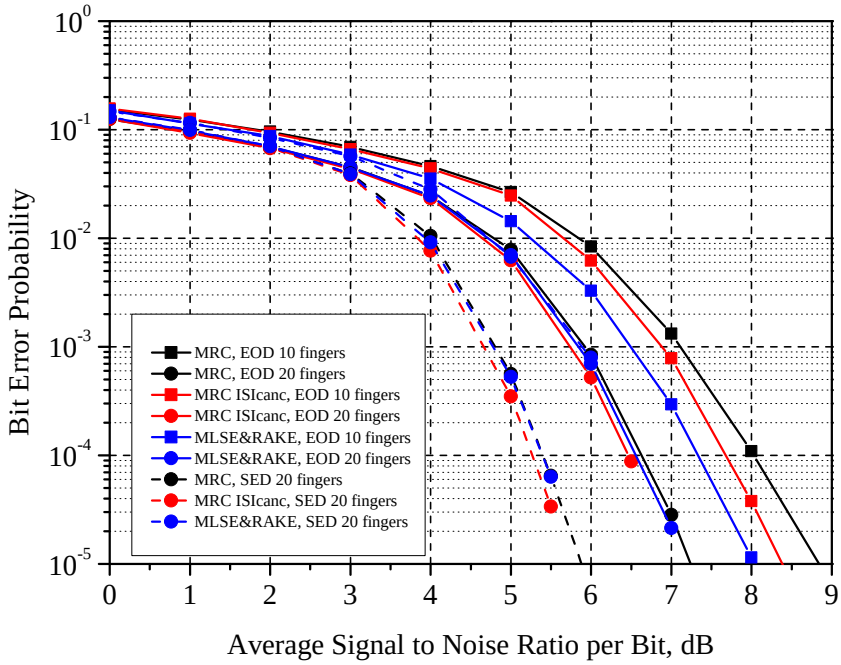

Figure 5.5: BEP over NLOS industrial environment CM8 of different receivers with different number of fingers N_R.

For the SED cases and a BEP in the order of 10^{-4} the gain attained for all the receivers for $\Lambda_R = 20$ is 1 dB. As mentioned above, the addition of the optimum SED manages to lower the BEP for every receiver, where they all achieve the same BEP.

Chapter 6

Conclusion and future work

6.1 Conclusions

We analyzed the performance of IEEE 802.15.4 UWB PHY high rate mode over realistic residential, office, outdoor and industrial environments. We evaluated the performance of the proposed scheme with MRC, MRC with ISI cancellation and MLSE & RAKE combination receiver, with the addition of optimal erasures decoding over fading channels.

Apart from the statistical analysis we verified that the sRAKE receiver is a definite plus on all the situations and that the increase of fingers is mandatory in order to improve performance. Also with the simulation over outdoor LOS environment, which is the highest delay spread for the LOS environments, we proved there is no point on simulating over the LOS environments.

In the residential environment we found that for a low number of sRAKE fingers ISI mitigation gain exists but it is low, while for a high number of fingers the MRC diversity outperforms the MLSE & RAKE combination receiver. On the other hand, in the office environment with the least delay spread we found that ISI mitigation can still give a small gain in a low number of sRAKE finger, while for a high number of sRAKE fingers the BEP performance for all receivers is pretty much the same.

The outdoor environment with the highest delay spread environment showed that ISI mitigation is required for a low number of sRAKE fingers and can provide a gain even at a high number of sRAKE fingers. This is the only environment where the MLSE & RAKE combination receiver manages to outperform the other receivers regarding the BEP performance. A special attention must be given into the fact that we can see a difference in the BEP performance when 1 or 2 previous symbols are removed through the ISI estimation. For the industrial environment we found that for a low number of sRAKE fingers the gain of ISI mitigation techniques can be high, while for a high number of sRAKE fingers all the receivers give the same BEP performance.

In any environment optimal errors and erasures decoding can provide a further gain of at least 1 dB in the BEP performance. Specially for the outdoor environment the gain can go further up to 1.5 dB. Overall in cases of low number of finger the ISI mitigation techniques can provide a gain in all environment. In cases with high number of fingers the received power is increases the diversity of the MRC

and helps to improve performance and ISI mitigation receivers can still provide a negligible gain.

6.2 Future work

Further improvements could include the customization of channel parameters, like the addition of antenna gains, frequency dependence of path gains, shadowing or large-scale fading and distance dependence of the pathloss. This will allow to simulate the expected BEP over distance for each environment and build specific receiver according to the environment needs. More information regarding the way of application can be found in [2].

Another idea is combining the MRC diversity gains with the MLSE & RAKE ability to mitigate interference in high ISI environments. The MRC receiver has proven to perform well in cases that the capture energy by the RAKE fingers is significant to the total received energy. In the case of a high delay profile environment like outdoor were the RAKE captured energy is low and ISI is high, a possible combination of the two receivers would provide an optimal implementation however with increased complexity.

Finally it would be interesting the application of block Decision Feedback Equalization (DFE) [22]. Many papers can be found in literature regarding DFE but specifically in [23] we can see a generalized MLSE arbitration for High Speed Packet Access (HSPA) Wideband Coded Division Multiple Access (WCDMA). Original block equalization involves joint detection of symbols from an overall symbol period and the use of a feedback filter in order to remove the interference from that past symbol period. They extend the idea to parallel symbol streams, add feedforward filtering and introduce a notion of block linear equalization. Been able to work in a codeword level to remove the ISI will provide more effective power to the MRC receiver, which will perform better with the maximum diversity.

References

[1] IEEE 802.15.4-2011, "IEEE Standard for Local and Metropolitan Area Networks–Part 15.4: Low-Rate Wireless Personal Area Networks (LR-WPANs)," New York, NY, USA, IEEE, Sep. 2011.

[2] A. Molisch et al., "A comprehensive standardized model for ultrawideband propagation channels," IEEE Trans. Antennas and Propag., vol. 54, no. 11, pp. 3151–3166, Nov. 2006.

[3] Z. Ahmadian and L. Lampe, "Performance analysis of the IEEE 802.15.4a UWB system," IEEE Trans. Commun., vol. 57, no. 5, pp. 1474–1485, May 2009.

[4] S. Kim, Y. Kim, X. Li, and J. Kang, "Orthogonal pulse design in consideration of FCC and IEEE 802.15.4a constraints." IEEE Commun. Letters, vol. 17, no. 5, pp. 896–899, May 2013.

[5] I. Dotlic and R. Kohno, "Low complexity chirp pulsed ultra-wideband system with near-optimum multipath performance," pp. 208–218, Jan. 2011.

[6] S. Ji, S. Lee, and J. Kim, "Efficient hybrid modulation with phase-directed pulse position estimation for UWB-IR systems." IEEE Trans. Commun., vol. 61, no. 3, pp. 1171–1177, Mar. 2013.

[7] I. Dotlic and R. Miura, "Novel trellis coded modulation for coherent IEEE 802.15.4a impulse-radio ultra-wideband communications," in Proc. IEEE International Conference on Intelligent Sensors, Sensors Networks and Information Processing (ISSNIP'14), Singapore, Apr. 2014, pp. 1–6.

[8] L. Reggiani and G. Maggio, "Orthogonal convolutional modulation for uwb-impulse radio systems: performance analysis and adaptive schemes," Wireless Communications, IEEE Transactions on, vol. 8, no. 9, pp. 4550–4560, September 2009.

[9] D. Cassioli, M. Win, F. Vatalaro, and A. Molisch, "Low complexity rake receivers in ultra-wideband channels," Wireless Communications, IEEE Transactions on, vol. 6, no. 4, pp. 1265–1275, April 2007.

[10] S. Wang, Y. Chen, M. Leeson, and N. Beaulieu, "New receivers for generalized uwb transmitted reference systems with improved performances," Wireless Communications, IEEE Transactions on, vol. 9, no. 6, pp. 1837–1842, June 2010.

[11] H. Shao and N. Beaulieu, "An analytical method for calculating the bit error rate performance of rake reception in uwb multipath fading channels," Communications, IEEE Transactions on, vol. 58, no. 4, pp. 1112–1120, April 2010.

[12] P. Kaligineedi and V. K. Bhargava, "A chip-rate MLSE equalizer for DS-UWB systems," in Proc. National Conference on Communications (NCC'06), New Delhi, India, Jan. 2006, pp. 78–82.

[13] X. N. S. Yang, Q. Yin and Z. Li, "A DS-UWB interpath interference suppression scheme based on MLSE algorithm," in Proc. International Conference on Signal Processing (ICSP) 2006), Beijing, China, Nov. 2006, pp. 1–3.

[14] M. Eslami and X. Dong, "Rake-MMSE-equalizer performance for UWB," IEEE Commun. Letters, vol. 9, no. 6, pp. 502–504, June 2005.

[15] N. Boubaker and K. B. Letaief, "Mmse multipath diversity combining for multi-access th-uwb in the presence of nbi." IEEE Transactions on Wireless Communications, vol. 5, no. 4, pp. 712–719, 2006.

[16] F. Troesch and A. Wittneben, "Low power UWB transceivers for isi limited environments: Design and performance verification," in Proc. IEEE International Conference on Ultra-Wideband (ICUWB) 2009, Vancouver, Canada, Sep. 2009, pp. 269–273.

[17] S. Jamali, N. Le, and T. Le-Ngoc, Coded-Modulation Techniques for Fading Channels, ser. Kluwer international series in engineering and computer science: Communications and information theory. Springer US, 1994.

[18] S.-W. Lee and B. V. K. V. Kumar, "Soft-decision decoding of Reed-Solomon codes using successive error-and-erasure decoding," in Proc. IEEE Global Telecommunications Conference (GLOBECOM) 2008, New Orleans, LO, USA, Dec. 2008, pp. 1–5.

[19] M. Di Benedetto, UWB Communication Systems: A Comprehensive Overview. Hindawi Publishing Corporation, 2006.

[20] S. Kim, Y. Kim, X. Li, and J. Kang, "Orthogonal pulse design in consideration of fcc and ieee 802.15.4a constraints," Communications Letters, IEEE, vol. 17, no. 5, pp. 896–899, may 2013.

[21] J. Proakis and M. Salehi, Digital Communications, ser. McGraw-Hill higher education. McGraw-Hill Education, 2007.

[22] D. Williamson, R. Kennedy, and G. Pulford, "Block decision feedback equalization," Communications, IEEE Transactions on, vol. 40, no. 2, pp. 255–264, Feb 1992.

[23] G. Bottomley, "Block equalization and generalized mlse arbitration for the hspa wcdma uplink," in Vehicular Technology Conference, 2008. VTC 2008-Fall. IEEE 68th, Sept 2008, pp. 1–5.

LUND
UNIVERSITY

Series of Master's theses
Department of Electrical and Information Technology
LU/LTH-EIT 2015-452

http://www.eit.lth.se